INSTITUTE FOR FUSION STUDIES

DOE/ET-53088-560 IFSR #560

Nonlinear Studies of $m = 1$ Modes in High-Temperature Plasmas

A.Y. AYDEMIR
Institute for Fusion Studies
The University of Texas at Austin
Austin, Texas 78712

July 1992

THE UNIVERSITY OF TEXAS

AUSTIN

Nonlinear Studies of $m = 1$ Modes in High-Temperature Plasmas

A.Y. Aydemir
Institute for Fusion Studies
The University of Texas at Austin
Austin, Texas 78712

Abstract

Nonlinear evolution of the $m = 1$ mode is examined in high-temperature plasmas where the mode is in the semi-collisional or collisionless regime. Unlike the resistive $m = 1$ mode, both the semi-collisional mode, with a very weak resistivity dependence, and the collisionless mode, driven by finite electron inertia, can be robustly unstable in today's large tokamaks. And unlike the finite-$\Delta'(m \geq 2)$ tearing modes, the nonlinear evolution of which is collisional, both the semi-collisional and collisionless $m = 1$ modes exhibit nonlinearly enhanced growth rates that far exceed their linear values, thus making their nonlinear evolution collisionless; this accelerated growth of a collisionless $m = 1$ mode may explain the fast sawtooth-crashes observed in large tokamaks.

PACS No's: 52.35.Py, 52.30.Jb, 52.55.Fa, 52.35.Dm.

Because of its relevance to understanding and controlling the sawtooth oscillations in tokamaks, the $m = 1$ mode continues to receive a great deal of attention. The nonlinear evolution of the $m = 1$ mode was first examined by Rosenbluth *et al.*,[1] in an ideal magnetohydrodynamic (MHD) context, where it was found to saturate with a small amplitude. Later, Kadomtsev[2] offered a heuristic argument about the nonlinear evolution of the resistive $m = 1$ as an explanation for the sawtooth oscillations.[3] More formally, the nonlinear evolution of the $m = 1$ was examined in a resistive MHD context by Hazeltine *et al.*,[4] Waelbroeck,[5] and Biskamp,[6] elucidating the differences between $m = 1$, and $m \geq 2$ tearing modes, which nonlinearly enter a "Rutherford regime."[7] Recently, Zakharov[8] has extended the nonlinear analysis to two-fluid regime, finding good agreement between his nonlinear estimates of the sawtooth crash times and experimental observations.

In this letter, we present nonlinear computational results, using essentially a two-fluid theory based on the four-field model of Hazeltine *et al.*,[9] in which the $m = 1$, in the high-temperature regime where the mode is either semi-collisional or collisionless, exhibits a novel behavior: nonlinearly, the growth rate increases dramatically, thus offering an alternative explanation for the fast sawtooth crashes. This computational result does not seem to have been predicted by any of the analytic nonlinear theories mentioned above; this behavior of the $m = 1$ mode, where the mode growth accelerates, and it is pushed into the collisionless regime, even if it is not there linearly, also differs from the nonlinear evolution of $m \geq 2$ semicollisional and collisionless tearing modes, which nonlinearly slow down and become collisional.[10]

The four-field model[9] used in this work, although it is based on a reduced MHD description and lacks some of the geometrical effects of full MHD calculations that are commonplace now, is a simplified model of tokamak dynamics that includes finite-Larmor-radius (FLR) effects, diamagnetic drift frequencies, and the effects of long-mean-free-path electron dynam-

ics. In an earlier work, it was shown to reproduce many of the well-known dispersion relations for the $m = 1$ mode in collisional, semi-collisional, and collisionless regimes.[11] Omitting the curvature terms, and including terms due to finite electron inertia in the parallel Ohm's law, the equations for a generalized vorticity U, flux function ψ, electron pressure p, and the parallel ion velocity v, respectively, can be written in the form

$$\frac{\partial U}{\partial t} + [\phi, U] + \nabla_{\|} J = \delta\tau \nabla_{\perp} \cdot [p, \nabla_{\perp}\phi] \ , \tag{1}$$

$$\frac{\partial \psi}{\partial t} + \nabla_{\|} [\phi - (1+\tau)\delta p] = \eta J + \delta_s^2 \left\{ \frac{\partial J}{\partial t} + [\phi - \delta\tau p, J] \right\} \ , \tag{2}$$

$$\frac{\partial p}{\partial t} + [\phi, p] + \beta \nabla_{\|} [v + 2\delta J] = 0 \tag{3}$$

$$\frac{\partial v}{\partial t} + \frac{1}{2}(1+\tau)\nabla_{\|} p + [\phi - \delta\tau p, v] = 0 \ , \tag{4}$$

$$\phi = \phi_{\text{elect}} + \delta\tau p \ , \tag{5}$$

$$J = \nabla_{\perp}^2 \psi \ , \qquad U = \nabla_{\perp}^2 \phi \ , \qquad \tau = \frac{T_i}{T_e} \ , \tag{6}$$

$$\beta = \frac{nkT_e}{B_T^2/2\mu_o} \quad \delta = \frac{c/2\omega_{pi}}{a} \ , \quad \delta_s = \frac{c/\omega_{pe}}{a} = 2\left(\frac{m_e}{m_i}\right)^{1/2} \delta \ . \tag{7}$$

The variables have been normalized as follows: $t \rightarrow t/\tau_{Hp}$, $\mathbf{r} \rightarrow \mathbf{r}/a$, $\eta = \tau_{Hp}/\tau_R$, where $\tau_{Hp} = a/u_{Hp}$, $\tau_R = \mu_o\, a^2/\eta_o$, and $u_{Hp} = B_{po}^2/\sqrt{\rho_o \mu_o}$. τ_{Hp} and τ_R are the poloidal Alfvén time and the resistive diffusion time, respectively, defined in terms of the minor radius a, a characteristic poloidal field strength B_{po}, and resistivity η_o.

The brackets are defined by $[\phi, U] = \hat{\zeta} \cdot \nabla_{\perp}\phi \times \nabla_{\perp} U$, where $\hat{\zeta}$ is a unit vector in the toroidal direction, and $\nabla_{\perp}$ is the 2-D gradient in the plane perpendicular to the magnetic field. The parallel gradient operator is defined as $\nabla_{\|} J = \partial J/\partial\zeta + [J, \psi]$ for any scalar J. The parameter δ, in combination with the electron β, is related to the ion Larmor radius,

as it can be shown that $\tau\delta^2\beta = (\rho_i/2)^2$. Similarly, the ion Larmor radius based on electron temperature, ρ_s, is defined by $(\rho_s/2)^2 = \delta^2\beta$. Both ρ_i and ρ_s are normalized to the minor radius. Finally, δ_s is the collisionless skin depth.

With the finite-electron-inertia terms present, it turns out to be more convenient to rewrite the parallel Ohm's law in terms of an auxiliary variable $\chi \equiv \psi - \delta_s^2 J$, which gives

$$\frac{\partial \chi}{\partial t} + [\phi - \delta\tau p \ , \ \chi] + \frac{\partial}{\partial \zeta}(\phi - \delta\tau p) = \delta \nabla_{\|} p + \eta J + \mu_e \nabla_{\perp}^2 \chi \ . \tag{8}$$

Note that we have included an electron viscosity term on the right-hand side, which leads to an effective resistivity of $\eta_{\text{effec}} = \eta + \mu_e$, and a hyperresistivity of $\eta_{\text{hyper}} = \mu_e \delta_s^2$. Since the effects of hyperresistivity were examined in an earlier work,[12] we will not consider it further and keep $\mu_e \ll \eta$ here.

Using $\eta_0 = m_e \nu_{ei}/2e^2 n_e$, where ν_{ei} is the electron-ion collision frequency, and defining a resistive layer width, $x_\eta^2 = \eta/\omega$, it can be shown that Drake and Lee's semicollisional regime[13] corresponds to $\delta_s < x_\eta < \delta$ in the four-field model; the collisionless regime is obviously given by $x_\eta < \delta_s$.

The nonlinear increase in the growth rate of the $m = 1$ mode is observed in both semicollisional regime, where the electron inertia terms in the parallel Ohm's law can be ignored ($x_\eta \gg \delta_s$), and in the collisionless regime where the electron inertia term dominates over the collisional effects ($x_\eta \ll \delta_s$). For brevity, these two regimes will not be examined separately in this letter. We also let $\tau \equiv T_i/T_e = 0$, which removes, among others, the ion gyro-viscosity term on the right-hand side of the vorticity equation, Eq. (1); these terms do not seem to play a significant role in the stated nonlinear behavior of the mode. For consistency, the ion-sound terms, which come in through Eq. (4), are retained, although their effect was shown to be unimportant,[11] at least linearly.

The four-field equations, Eqs. (1)-(4), are solved in a cylindrical geometry, with periodically identified ends. The variables are Fourier-expanded in poloidal and toroidal directions;

pseudo-spectral techniques are used,[14] keeping up to 256 modes. In the radial direction, a nonuniform grid with over 600 grid-points is used. In order to reduce the oscillatory behavior of fields near regions with sharp gradients, a third-order upwind-biased differencing is used for the convective derivatives.

The most significant point of this letter is summarized in Fig. 1, which shows the time evolution of the growth rate of the mode, defined as $\gamma = (1/2)d\log E_K/d\log t$, where E_K is the total kinetic energy in the system. Some of the important parameters for this run were $\delta = 0.107$, $\delta_s = 5 \times 10^{-3}$, $\beta = 5 \times 10^{-3}$, and $\eta = 1.0 \times 10^{-6}$, which gave a linear growth rate of $\gamma = 1 \times 10^{-2}$. The dramatic increase in the growth rate of the mode as the island grows, which is not observed in a purely resistive calculation, is quite evident Fig. 1. The mode starts linearly in the semi-collisional regime ($\delta_s < x_\eta < \delta$) and becomes collisionless during the fastest part of the reconnection. The collisionless physics, provided by the electron inertia terms in the Ohm's law, however, is not essential to this accelerated growth; the same behavior is observed in a purely semi-collisional run where we set the collisionless skin depth, δ_s, to zero. Internal consistency, of course, requires that the electron inertia terms be kept for modes growing on this rapid time scale, as the classical resistive layer width becomes less than the collisionless skin depth.

Further differences between the semicollisional/collisionless mode and its purely resistive counterpart can be seen also in the geometry of the island and the current sheet that develops around the separatrix. Figure 2 shows the helical flux contours associated with the nonlinear run of Fig. 1, at four points during the nonlinear evolution of the island, pointed at with arrows in Fig. 1. The early nonlinear behavior is similar to that of a purely resistive island; the reconnection layer is poloidally extended and forms more of a "Y-point"[5, 6] than the classical X-point of an $m \geq 2$-island. However, as the island grows further, a well-defined X-point emerges, widening the outflow region of the reconnection layer. The accelerated growth (faster reconnection) can be attributed to this change in the geometry of the layer,

as it is certainly easier to remove the reconnected flux with a "wider nozzle." Figure 3 shows the contours of the current density, at the same times as the flux contours of Fig. 2. Again the change in the geometry is clear; the extended current sheet of the 'Y-layer' of early times breaks up and forms an "X-layer," clearly following the contours of the island separatrix. The current sheet that forms at the inner separatrix of the island shrinks and disappears as reconnection approaches completion; the sheet along the outer separatrix lengthens and eventually extends all the way around the circle, as predicted by Kadomtsev.[2]

For comparison, Fig. 4 shows the flux and current contours from a highly nonlinear stage of a purely resistive $m = 1$ island; the presence of two "Ypoints," and an extended current sheet with a clearly different geometry from those of Fig. 3 are quite evident.

This novel behavior exhibited by the semicollisional/collisionless $m = 1$ mode can be traced to the coupling between the electron pressure gradient term in the Ohm's law, Eq. 2, and the parallel divergence of the electron velocity $(v + 2\delta J)$ in Eq. 3; linearly, these terms give rise to an adiabatic electron response in the long mean-free-path regime. The exact nonlinear mechanism that gives rise to an increase in the growth rate, however, is not clear at this point.

For computational economy, in the calculations presented above, rather unrealistic, but internally consistent, set of parameters were used. In a large tokamak, we typically find: the "FLR parameter" of the four-field model, $\delta \sim \mathcal{O}(10^{-2})$, the collisionless skin depth, $\delta_s \sim \mathcal{O}(10^{-3})$, and the resistivity $\eta < 10^{-8}$, in normalized units. The $m = 1$ mode exhibits the same nonlinear behavior under more realistic conditions; although calculations with exact experimental parameters are difficult, scaling studies with varying values of δ_s, δ, etc. are underway and will be presented in a longer article in the future.

In summary, the nonlinear evolution of the $m = 1$ mode in high temperature plasmas is found to be quite different from what is expected from a purely resistive MHD picture. In particular, allowing for an adiabatic electron response seems to lead nonlinearly to a

dramatic increase in the growth rate of the mode and in the rate of reconnection. The current sheet with its characteristic "Y" shape seen in resistive calculations, and also in the early stages of the nonlinear semicollisional/collisionless modes, quickly develops an "X-point" geometry. Concomitant with this change in the geometry of the reconnection layer, the growth rate of the mode increases, resulting in a rapid reconnection of the remaining flux. Although this process, because of its fast time scale, is collisionless, the collisionless physics introduced with finite electron inertia terms in the Ohm's law are not responsible for this change in the reconnection layer geometry or its rate. The accelerated growth of the semicollisional/collisionless $m = 1$ mode may explain the fast sawtooth crash times, although this conclusion needs further confirmation by scaling studies into more realistic parameter regimes.

Acknowledgments

Useful discussions with R.D. Hazeltine are gratefully acknowledged. This work was supported by the U.S. Department of Energy contract No. DE-FG05-80ET-53088.

References

[1]M.N. Rosenbluth, R.Y. Dagazian, and P.H. Rutherford, Phys. Fluids **16**, 1894 (1973).

[2]B.B. Kadomtsev, Fiz. Plazmy **1**, 710 (1975) [Sov. J. Plasma Phys. **1**, 389 (1975)].

[3]S. von Goeler, W. Stodiek, and N. Sauthoff, Phys. Rev. Lett. **33**, 1201 (1974).

[4]R.D. Hazeltine, J.D. Meiss, and P.J. Morrison, Phys. Fluids **29**, 1633 (1986).

[5]F.L. Waelbroeck, Phys. Fluids B **1**, 2372 (1989).

[6]Dieter Biskamp, Phys. Fluids B **3**, 3353 (1991).

[7]P.H. Rutherford, Phys. Fluids **16**, 1903 (1973).

[8]L.E. Zakharov, "Two-Fluid Magnetohydrodynamic Description of the Internal Kink Mode in Tokamaks," submitted to Phys. Fluids B (1992).

[9]R.D. Hazeltine, C.T. Hsu, and P.J. Morrison, Phys. Fluids **30**, 3204 (1987).

[10]J.F. Drake and Y.C. Lee, Phys. Rev. Lett. **39**, 453 (1977).

[11]A.Y. Aydemir, Phys. Fluids B **3**, 3025 (1991).

[12]A.Y. Aydemir, Phys. Fluids B **2**, 2135 (1990).

[13]J.F. Drake and Y.C. Lee, Phys. Fluids **20**, 1341 (1977).

[14]S.A. Orszag, Numerical Analysis of Spectral Methods: Theory and Analysis, Philadelphia, (1977).

Figure Captions

1. The growth rate as a function of time for an $m = 1$ mode that starts in the semicollisional regime and exhibits a dramatic increase in its growth rate, becoming collisionless during its nonlinear evolution. Time and the growth rate are normalized to the poloidal Alfvén time. The arrows point to approximate points in time where the flux function and current density contours are shown in subsequent figures.

2. The contours of the helical flux function at various points during the nonlinear evolution of the semicollisional $m = 1$ mode, the growth rate of which is shown in Fig. 1.

3. The current density contours for the semicollisional $m = 1$ mode, showing the change in the geometry of the current sheet from a flat ribbon (Y-layer) to a well-defined X-point.

4. Flux function and current density contours for a purely resistive $m = 1$ island, showing the typical Y-point geometry of the current layer on the separatrix, shown here for comparison with the semicollisional island of Figs. 3 and 4.

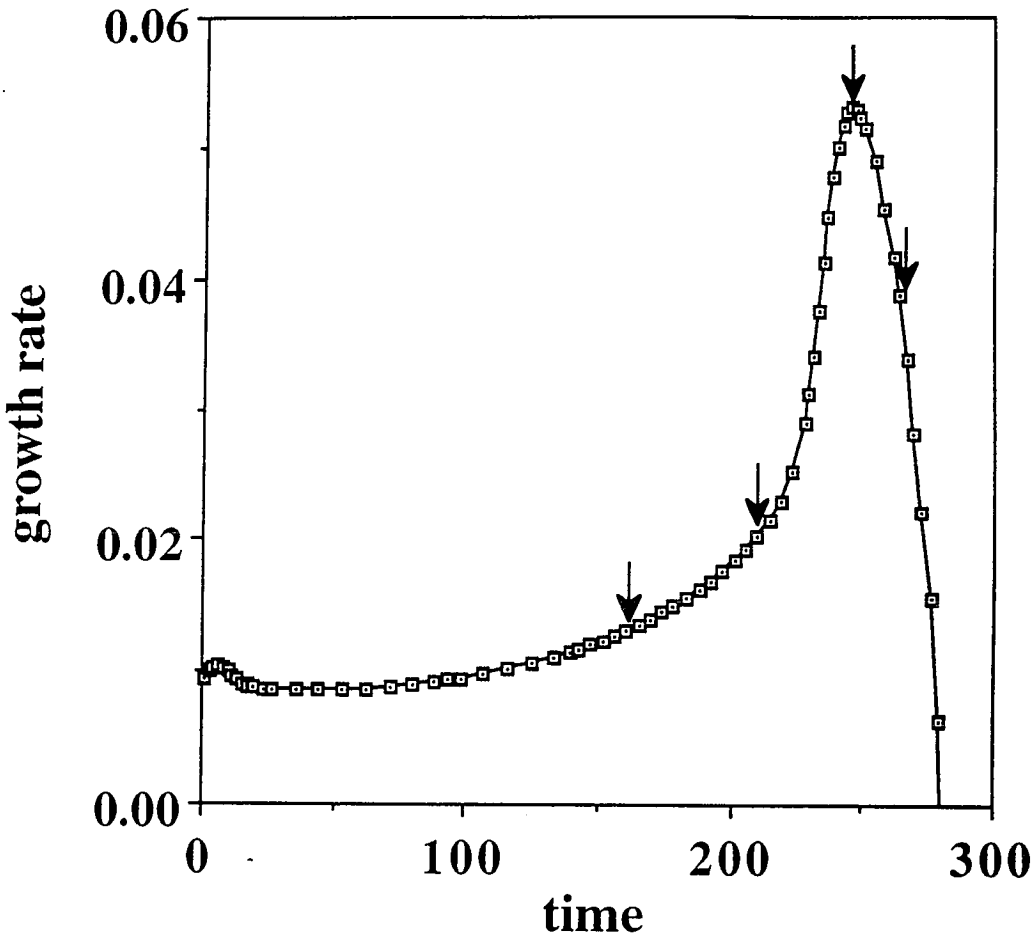

Fig. 1

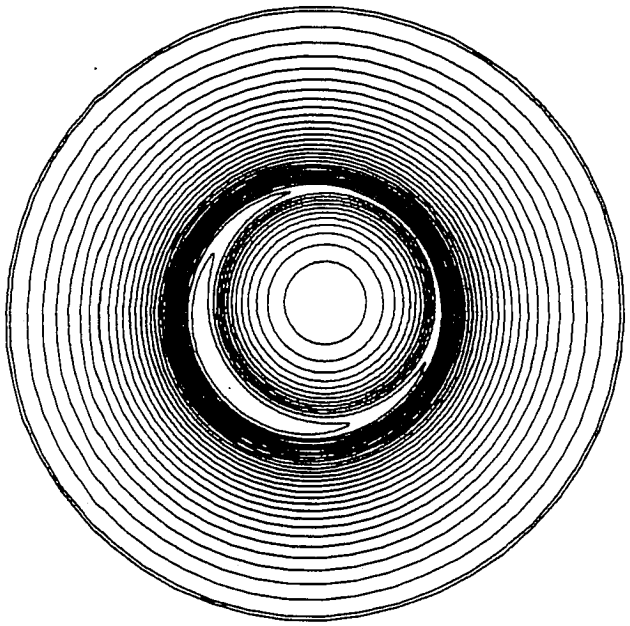

t= 1.60726E+02 HELICAL FLUX

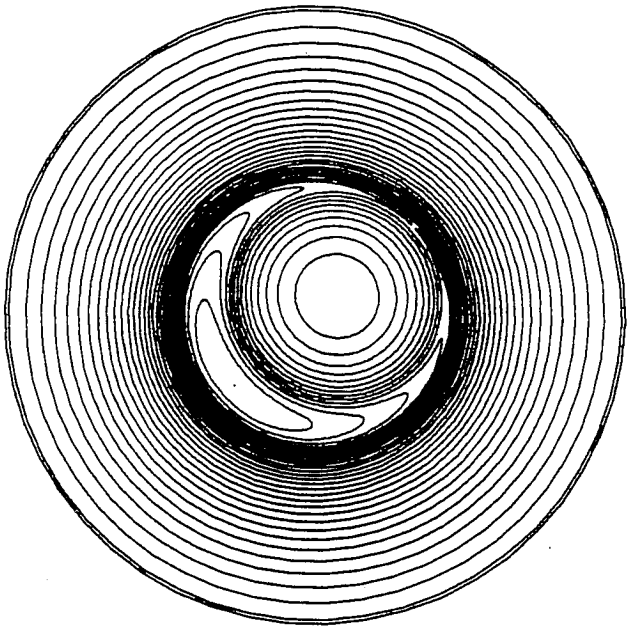

t= 2.14289E+02 HELICAL FLUX

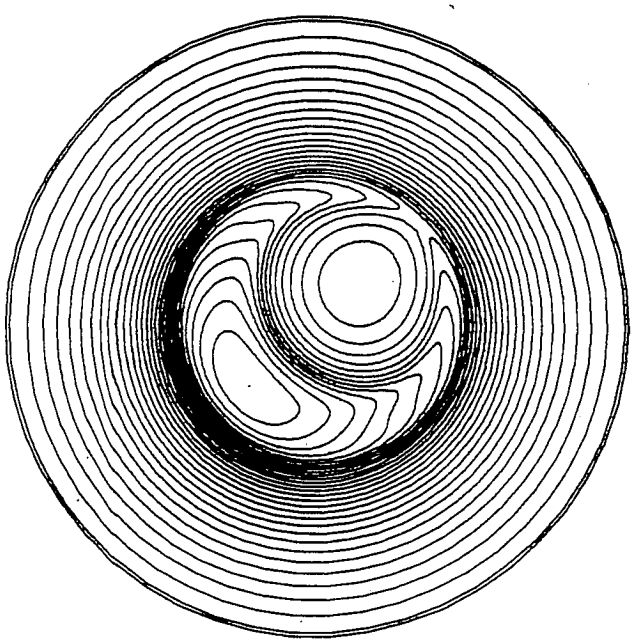

t= 2.49998E+02 HELICAL FLUX

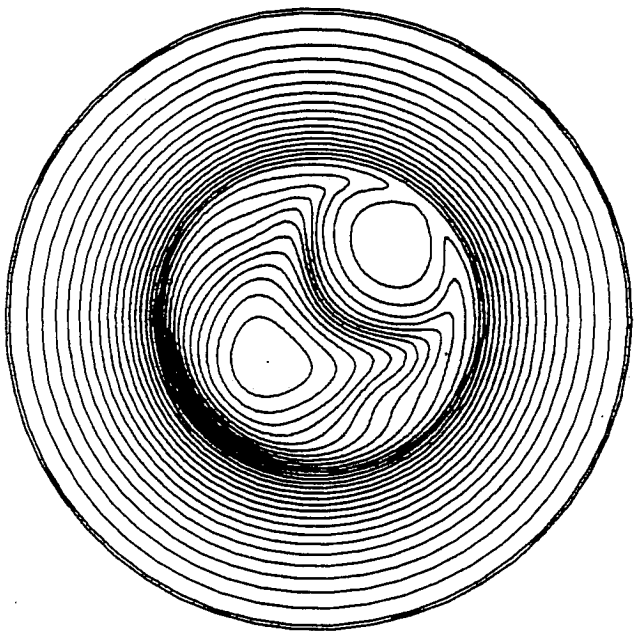

t= 2.64152E+02 HELICAL FLUX

Fig. 2

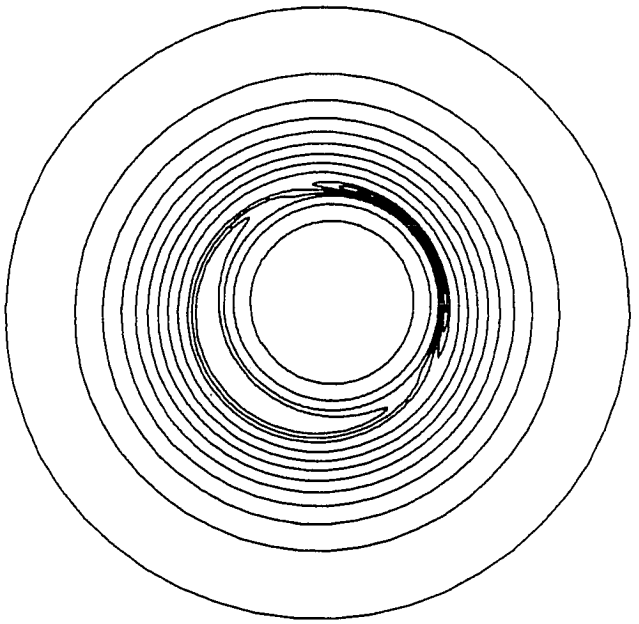

t= 1.60726E+02 TOROIDAL CURRENT

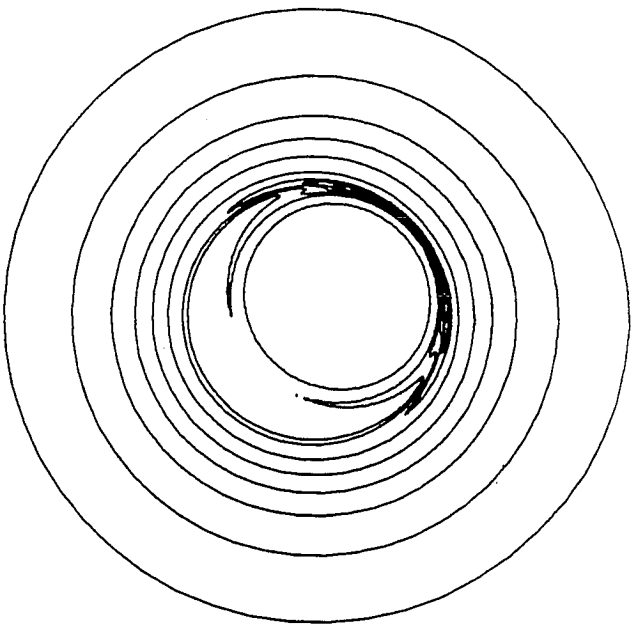

t= 2.14289E+02 TOROIDAL CURRENT

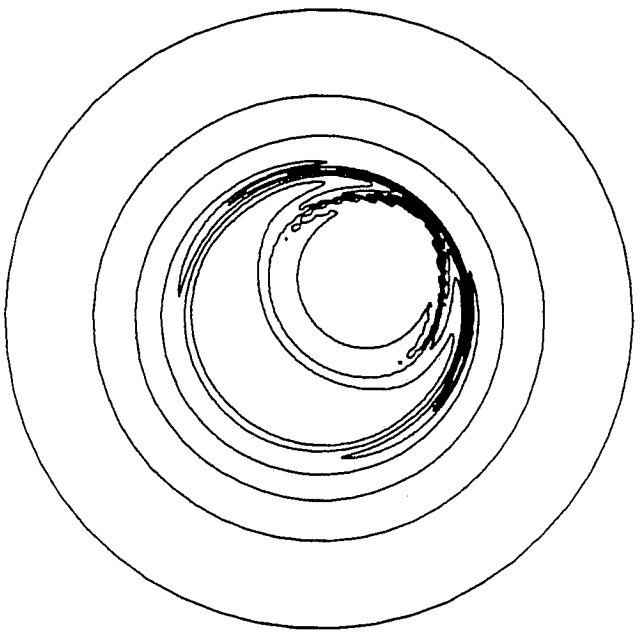

t= 2.49998E+02 TOROIDAL CURRENT

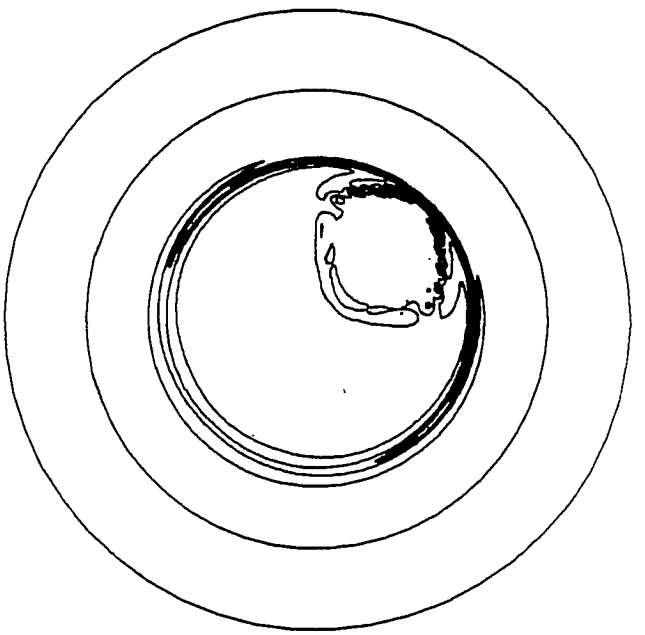

t= 2.64152E+02 TOROIDAL CURRENT

Fig. 3

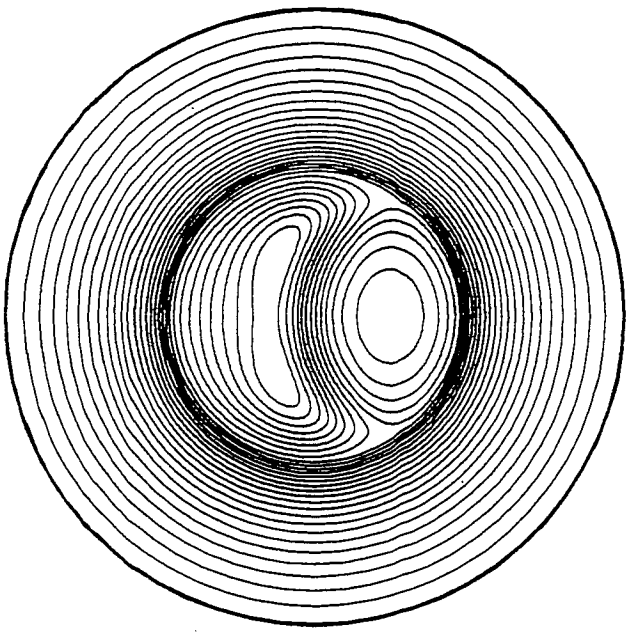

t= 4.28467E+02 HELICAL FLUX

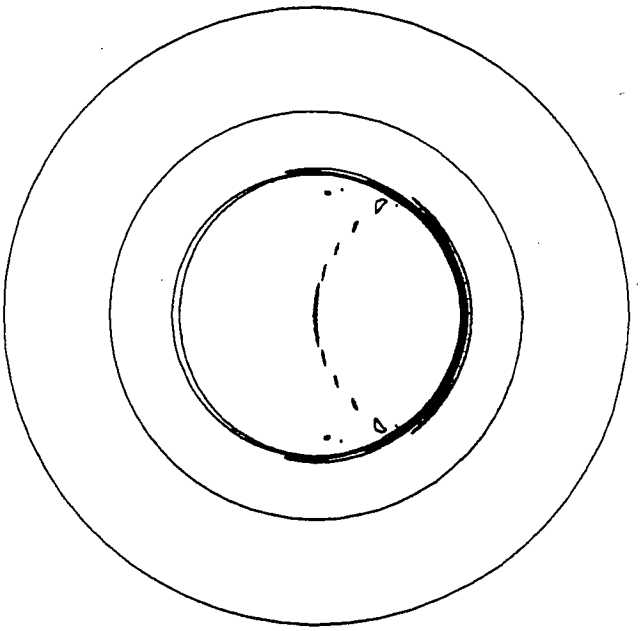

t= 4.28467E+02 TOROIDAL CURRENT

Fig. 4